

How Low Can We Go: Trading Memory for Error in Low-Precision Training

Chengrun Yang^{*1}, Ziyang Wu^{*1}, Jerry Chee¹, Christopher De Sa¹, Madeleine Udell¹

Abstract

Low-precision arithmetic trains deep learning models using less energy, less memory and less time. However, we pay a price for the savings: lower precision may yield larger round-off error and hence larger prediction error. As applications proliferate, users must choose which precision to use to train a new model, and chip manufacturers must decide which precisions to manufacture. We view these precision choices as a hyperparameter tuning problem, and borrow ideas from meta-learning to learn the tradeoff between memory and error. In this paper, we introduce Pareto Estimation to Pick the Perfect Precision (PEPPP). We use matrix factorization to find non-dominated configurations (the Pareto frontier) with a limited number of network evaluations. For any given memory budget, the precision that minimizes error is a point on this frontier. Practitioners can use the frontier to trade memory for error and choose the best precision for their goals.

1 Introduction

Training modern-day neural networks is becoming increasingly expensive as task and model sizes increase. The energy consumption of the corresponding computation has increased alarmingly, and raises doubts about the sustainability of modern training practices [1]. Low-precision training can reduce consumption of both computation [2] and memory [3], thus minimizing the cost and energy to train larger models and making deep learning more accessible to resource-limited users.

Low-precision training replaces 32-bit or 64-bit floating point numbers with fixed or floating point numbers that allocate fewer bits for the activations, optimizers, and weights. A rich variety of methods appear in recent literature, including bit-centering [2], loss scaling [5] and mixed-precision training [6]. There is however a fundamental tradeoff: lowering the number of bits of precision increases the *quantization error*, which may disrupt convergence and increase downstream error [7, 8, 9]. The *low-precision configuration* is thus a hyperparameter to be chosen according to the resource constraints of the practitioner.

How should we choose this hyperparameter? Many believe the highest allowable precision (given a memory budget) generally produces the lowest error model. However, there are typically many ways to use the same amount of memory. As shown in Figure 1(a), some of these configurations produce

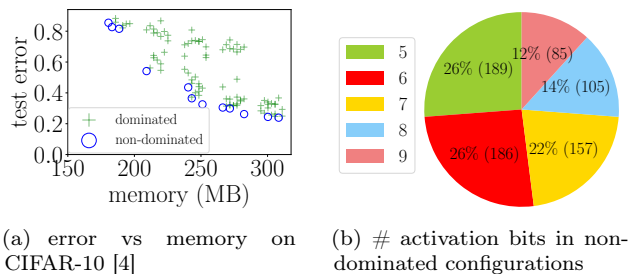


Figure 1: Test error vs memory for ResNet-18 across 99 low-precision floating point configurations. Figure (a) shows the tradeoff on CIFAR-10. (Non-dominated points are blue circles.) Figure (b) shows that the best precision to use varies depending on the memory budget, on 87 image datasets. See Section 4 for experimental details.

^{*}Equal contribution.

¹Cornell University, Ithaca, NY, USA. Email: {cy438, zw287, jc3464}@cornell.edu, cdesa@cs.cornell.edu, udell@cornell.edu.

much lower error than others! Figure 1(b) shows that no one configuration dominates all others. We might consult previous literature to choose a precision; but this approach fails for new applications.

Our goal is to efficiently pick the best low-precision configuration under a memory budget. Efficiency is especially important for resource-constrained practitioners, such as individual users or early-stage startups. To promote efficiency, we use a meta-learning [10, 11, 12] approach: we train a small number of cheap very-low-precision models on the dataset to choose the perfect precision. The gains from choosing the right low-precision format can offset the cost of this extra training — but each precision must be chosen carefully to realize the benefits of low-precision training.

We use ideas from multi-objective optimization to characterize the tradeoff between memory and error and identify the *Pareto frontier*: the set of non-dominated solutions. Users will want to understand the tradeoff between error and memory so they can determine the resources needed to adequately train a model for a given machine learning task. This tradeoff may also influence the design of application-specific low-precision hardware, with profound implications for the future [13].

Computing the Pareto frontier by training models for all low-precision configurations is expensive and unnecessary. Cloud computing platforms like Google Cloud and Amazon EC2 charge more for machines with the same CPU and double memory: 25% more on Google Cloud² and 100% more on Amazon EC2³ as of mid-June 2021. We use techniques from meta-learning to leverage the information from other low-precision training runs on related datasets. This approach allows us to *estimate* the Pareto frontier without evaluating all of the low-precision configurations.

Our system, Pareto Estimation to Pick the Perfect Precision (PEPPP), has two goals. The first goal is to find the Pareto frontiers of a collection of related tasks, and is called *meta-training* in the meta-learning literature. Meta-training requires a set of *measurements*, each collected by training and testing a neural network with a given precision on a dataset. This information can be gathered offline with a relatively large resource budget, or by crowdsourcing amongst the academic or open-source community. Still, it is absurdly expensive to exhaustively evaluate all measurements: that is, every possible low-precision configuration on every task. Instead, we study how to choose a subset of the possible measurements to achieve the best estimate. The second goal we call *meta-test*: using the information learned on previous tasks, how can we transfer that information to a new task to efficiently estimate its Pareto frontier? This goal corresponds to a resource-constrained individual or startup who wants to determine the best low-precision configuration for a new dataset.

Both meta-training and meta-test rely on matrix completion and active learning techniques to avoid exhaustive search: we make a subset of all possible measurements and predict the rest. We then estimate the Pareto frontier to help the user make an informed choice of the best configuration. We consider two sampling schemes: uniform and non-uniform sampling. Uniform sampling is straightforward. Non-uniform sampling estimates the Pareto frontier more efficiently by making fewer or even no high-memory measurements.

To the best of our knowledge, PEPPP is the first to study the error-memory tradeoff in low-precision training without exhaustive search. In analogous settings, meta-networks were used to prune or quantize [14, 15], and knowledge distillation has been used to construct low-precision networks [16].

Figure 2 shows a flowchart of PEPPP. The rest of this paper is organized as follows. Section 2 introduces notation and terminology. Section 3 describes the main ideas we use to actively sample configurations and approximate Pareto frontiers. Section 4 shows experimental results.

2 Notation and terminology

Low-precision formats. We use floating point numbers for low-precision training in this paper. As an example, Figure 3 shows an 8-bit floating point number with 3 exponent bits and 4 mantissa bits. A specific low-precision representation with a certain number of bits for each part is called a *low-precision*

²<https://cloud.google.com/ai-platform/training/pricing>

³<https://aws.amazon.com/ec2/pricing/on-demand>

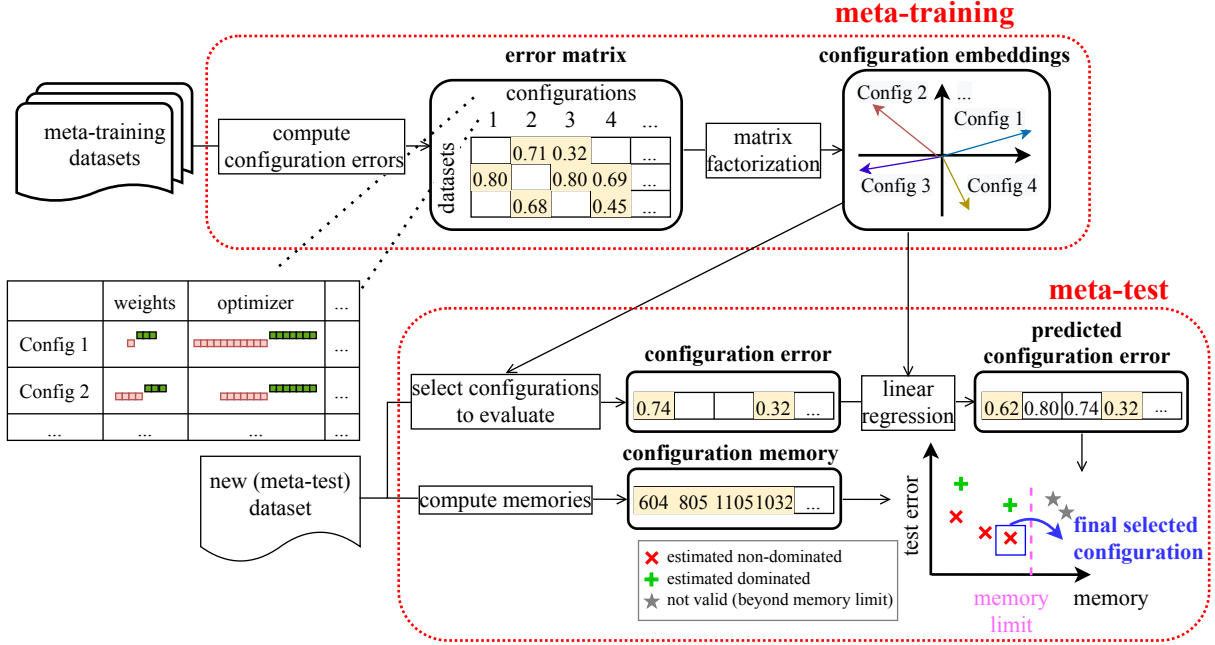


Figure 2: The PEPPP workflow. We begin with a collection of (meta-) training datasets and low precision configurations. In the meta-training phase, we sample dataset-configuration pairs to train, and compute the misclassification error. We use matrix factorization to compute a low dimensional embedding of every configuration. In the meta-test phase, our goal is to pick the perfect precision (within our memory budget) for the meta-test dataset. We compute the memory required for each configuration, and we select a subset of fast, informative configurations to evaluate. By regressing the errors of these configurations on the configuration embeddings, we find an embedding for the meta-test dataset, which we use to predict the error of every other configuration (including more expensive ones) and select the best subject to our memory budget.

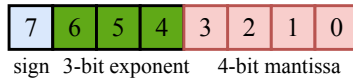


Figure 3: An 8-bit floating point number representing $(-1)^{\text{sign}} \cdot 2^{\text{exponent}-7} \cdot 1.b_3b_2b_1b_0$.

format. We may use different low-precision formats for the parameters, activations, and optimizer. In the case of using two formats to train and represent a neural network (as discussed in Section 3.1), these two formats are called *Format A* and *B*. A specific combination of these two formats is a hyperparameter setting of the neural network, and we call it a *low-precision configuration*.

Math basics. We define $[n] = \{1, \dots, n\}$ for a positive integer n . With a Boolean variable \mathcal{X} , the indicator function $\mathbf{1}(\mathcal{X})$ equals 1 if \mathcal{X} is true, and 0 otherwise. With a scalar variable x , we use x_+ to denote $\max\{x, 0\}$. \subseteq and \subset denote subset and strict subset, respectively.

Linear algebra. We denote vector and matrix variables respectively by lowercase letters (a) and capital letters (A). All vectors are column vectors. The Euclidean norm of a vector $a \in \mathbb{R}^n$ is $\|a\| := \sqrt{\sum_{i=1}^n a_i^2}$. To denote a part of a matrix $A \in \mathbb{R}^{n \times d}$, we use a colon to denote the varying dimension: $A_{i,:}$ and $A_{:,j}$ denote the i th row and j th column of A , respectively, and A_{ij} denotes the (i, j) -th entry. With an ordered index set $\mathcal{S} = \{s_1, \dots, s_k\}$ where $s_1 < \dots < s_k \in [d]$, we denote $A_{:\mathcal{S}} := [A_{:,s_1} \ \dots \ A_{:,s_k}] \in \mathbb{R}^{n \times k}$. Given two vectors $x, y \in \mathbb{R}^n$, $x \preceq y$ means $x_i \leq y_i$ for each $i \in [n]$. Given a matrix $A \in \mathbb{R}^{n \times d}$ and a set of observed indices as $\Omega \subseteq [n] \times [d]$, the partially observed matrix $P_\Omega(A) \in \mathbb{R}^{n \times d}$ has entries $(P_\Omega(A))_{ij} = A_{ij}$

		low-precision configurations						low-precision configurations			
		a	b	c	d			a	b	c	d
datasets	1	0.85	0.71	0.32	0.28	datasets	1	181	269	272	295
	2	0.80	0.80	0.80	0.69		2	180	269	272	295
	3	0.80	0.68	0.46	0.45		3	590	924	927	1032

(a) error matrix E (b) memory matrix M (MB)

Figure 4: Example error and memory matrices for some datasets and low-precision configurations. Dataset 1: CIFAR-10, 2: CIFAR-100 (fruit and vegetables), 3: ImageNet (stick) [18]. Configuration Format A (exponent bits, mantissa bits), Format B (exponent bits, mantissa bits). a: (3, 1), (6, 7); b: (3, 4), (7, 7); c: (4, 3), (8, 7); d: (5, 3), (6, 7).

if $(i, j) \in \Omega$, and 0 otherwise.

Pareto frontier. Multi-objective optimization simultaneously minimizes n costs $\{c_i\}_{i \in [n]}$. A feasible point $c^{(1)} = (c_1^{(1)}, \dots, c_n^{(1)})$ is *Pareto optimal* if for any other feasible point $c^{(2)} = (c_1^{(2)}, \dots, c_n^{(2)})$, $c^{(2)} \preceq c^{(1)}$ implies $c^{(2)} = c^{(1)}$ [17]. The set of Pareto optimal points is the *Pareto frontier*.

Tasks, datasets, measurements and evaluations. A *task* carries out a process (classification, regression, image segmentation, etc.) on a *dataset*. Given a deep learning model and a dataset, the training and testing of the model on the dataset is called a *measurement*. In our low-precision context, we *evaluate* a configuration on a dataset to make a measurement.

Meta-learning. Meta-learning transfers knowledge from past (*meta-training*) tasks to better understand the new (*meta-test*) task. To evaluate the error of meta-training, we use *meta-leave-one-out cross-validation* (meta-LOOCV): on a collection of tasks, each time we treat one task as meta-test and the others as meta-training, and average the results over all splits.

Error matrix and memory matrix. Given a neural network, the errors of different low-precision configurations on meta-training datasets form an *error matrix*, whose (i, j) -th entry E_{ij} is the test error of the j -th configuration on the i -th dataset. To compute the error matrix, we split the i -th dataset into training and test subsets (or use a given split), train the neural network at the j -th configuration on the training subset, and evaluate the test error on the test subset. The memory required for each measurement forms a *memory matrix* M , which has the same shape as the corresponding error matrix. Example error and memory matrices are shown in Figure 4.

3 Methodology

PEPPP operates in two phases: meta-training and meta-test. First in meta-training, we learn configuration embeddings by training a neural network of a specific architecture at different low-precision configurations on different datasets. As listed in Appendix A, we study image classification tasks and a range of low-precision formats that vary in the number of bits for the exponent and mantissa for the activations, optimizer, and weights. Our hope is to avoid enumerating every possible configuration since exhaustive search is prohibitive in practice. To this end, we make a few measurements and then predict the other test errors by active learning techniques. We also compute the memory matrix to understand the memory consumption of each measurement.

Then in meta-test, we assume that we have completed meta-training, and hence know the configuration embeddings. The meta-test goal is to predict the tradeoff between memory usage and test error on a new (meta-test) dataset. This step corresponds to inference in traditional machine learning; it must be quick and cheap to satisfy the needs of resource-constrained practitioners. To select the configuration that has smallest test error and takes less than the memory limit, we measure a few selected (informative and cheap) configurations on the meta-test dataset, and use the information of their test errors to predict the rest. The problem of choosing measurements is known as the “cold-start” problem in the literature on

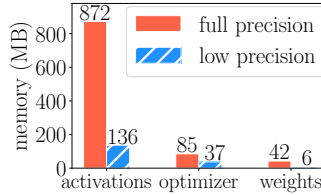


Figure 5: Memory usage under two training paradigms. Both train a ResNet-18 on CIFAR-10 with batch size 32.

recommender systems. Then we use the model built on the meta-training datasets to estimate values for the other measurements on the meta-test dataset.

3.1 Meta-training

On the n meta-training datasets, we first compute the memory needed to evaluate each of the d low-precision configurations to obtain the full memory matrix $M \in \mathbb{R}^{n \times d}$. The total memory consists of memory needed for model parameters, activations, and the optimizer (gradients, gradient accumulators, etc.) [19]. Among these three types of memory usage, activations typically dominate, as shown in Figure 5. Thus using lower precision for activations drastically reduces memory usage. Additionally, empirical studies [6] have shown that adopting higher precision formats for the optimizer can substantially improve the accuracy of the trained model. Since the optimizer usually requires a relatively small memory, it is often the best to use a higher precision format for this component. Thus for each low-precision configuration, it is typical to use a lower precision for network weights and activations, and a higher precision for the optimizer, resulting in combinatorially many choices in total. An example of the memory usage in this low-precision scenario is also shown in Figure 5.

In practice, ML tasks are often correlated: for example, meta-training datasets might be subsets of a large dataset like CIFAR-100 or ImageNet. The ranking of different configurations tends to be similar on similar tasks. For example, we computed the test errors of 99 low-precision configurations on 87 datasets (both listed in Appendix A) to form a performance vector in \mathbb{R}^{99} for each dataset. We use the Kendall tau correlation to characterize the alignment between the ranking of errors incurred by different configurations on two datasets: the Kendall tau correlation is 1 if the order is the same and -1 if the order is reversed. As shown in Figure 6(a), similar datasets have larger correlations: for example, datasets with indices 38–87 correspond to ImageNet subproblems such as distinguishing types of fruit or boat. Notice also that some dataset pairs have configuration performance rankings that are negatively correlated. The corresponding error matrix E concatenates the performance vector for each dataset. It is not low rank, but its singular values decay rapidly, as shown in Figure 6(b). Hence we expect low rank approximation of this matrix from a few measurements to work well: it is not necessary to measure every configuration.

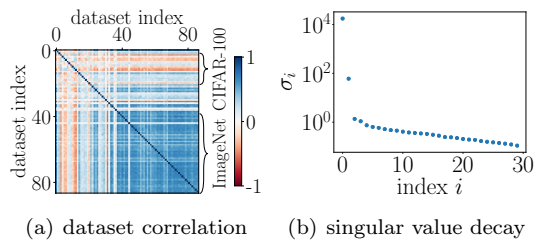


Figure 6: Kendall tau correlation of test error of all configurations between all pairs of datasets, and singular value decay of corresponding error matrix. Strong correlations allow PEPPP to succeed with a few measurements. Details in Appendix A.

In the uniform sampling scheme, we choose measurements to sample uniformly at random to obtain a partially observed error matrix $P_\Omega(E)$. We then estimate the full error matrix E using a low rank matrix completion method to form estimate \hat{E} . In this paper, we use SOFTIMPUTE [20, 21] (Algorithm 1, Appendix B). Using the estimated error matrix \hat{E} and computed memory matrix M , we compute the Pareto frontier for each dataset to understand the (estimated) tradeoff between memory and error. Section 4 Figure 10 shows an example.

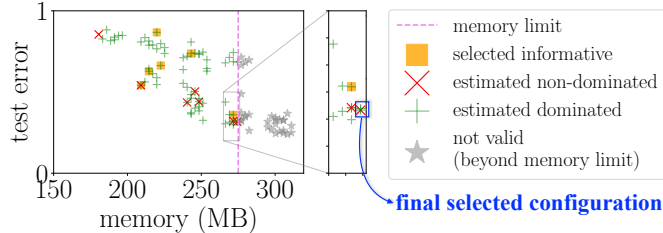


Figure 7: Meta-test on CIFAR-10. After meta-training on all other datasets in Appendix A Table 2, we use ED-MF to choose six informative measurements (orange squares) with a 275MB memory limit for each measurement on CIFAR-10. Then we estimate test errors of other configurations by ED-MF, and restrict our attention to configurations that we estimate to be non-dominated (red x’s). Note some of these are in fact dominated, since we plot true (not estimated) test error! Finally we select the estimated non-dominated configuration with highest allowable memory (blue square).

In the non-uniform sampling scheme, we choose measurements to sample with non-uniform probabilities, and use a weighted variant of SOFTIMPUTE, weighting by the inverse propensity score, to complete the error matrix [22]. Then we estimate the Pareto frontier in the same way as above. Non-uniform sampling is useful to reduce the memory needed for measurements. To this end, we construct a probability matrix P by entry-wise transformation $P_{ij} = \sigma(1/M_{ij})$, in which the monotonically increasing $\sigma : \mathbb{R} \rightarrow [0, 1]$ maps inverse memory usage to a sampling probability. In this way, we make more low-memory measurements, and thus reduce the total memory usage.

3.2 Meta-test

Having estimated the embedding of each configuration, our goal is to quickly compute the error-memory tradeoff on the meta-test dataset, avoiding the exhaustive search of all possible measurements.

We first compute the memory usage of each low-precision configuration on the meta-test dataset. With this information and guided by meta-training, we evaluate only a few (cheap but informative) configurations and predict the rest. Users then finally select the non-dominated configuration with highest allowable memory. An example of the process is shown in Figure 7.

PEPPP uses Experiment Design with Matrix Factorization (ED-MF) described below to choose informative configurations. With more time, ED-MF evaluates more configurations, improving our estimates. We may also set a hard cutoff on memory: we do not evaluate low-precision configurations exceeding the memory limit. This setting has been studied in different contexts, and is called *active learning* or *sequential decision making*.

ED-MF picks measurements to minimize the variance of the resulting estimate. Specifically, we factor a best rank- k approximation of the true (or estimated) error matrix $E \in \mathbb{R}^{n \times d}$ (or $\hat{E} \in \mathbb{R}^{n \times d}$) into dataset embeddings $X \in \mathbb{R}^{n \times k}$ and configuration embeddings $Y \in \mathbb{R}^{d \times k}$ as $E \approx X^T Y$ [23, 24]. On a meta-test dataset, we denote the error and memory vectors of the configurations as $e^{\text{new}} \in \mathbb{R}^d$ and $m^{\text{new}} \in \mathbb{R}^d$, respectively. We will model the error on the new dataset as $e^{\text{new}} = Y^T x^{\text{new}} + \epsilon \in \mathbb{R}^d$, where $x^{\text{new}} \in \mathbb{R}^k$ is the embedding of the new dataset and $\epsilon \in \mathbb{R}^d$ accounts for the errors from both measurement and low rank decomposition. We estimate the embedding x^{new} from a few measurements (entries) of e^{new} by least squares. Note that this requires at least k measurements on the meta-test dataset to make meaningful estimations, in which k is the rank for matrix factorization.

If $\epsilon \sim \mathcal{N}(0, \sigma^2 I)$, the variance of the estimator is $\left(\sum_{j \in S} y_j y_j^T \right)^{-1}$. D-optimal experiment design selects

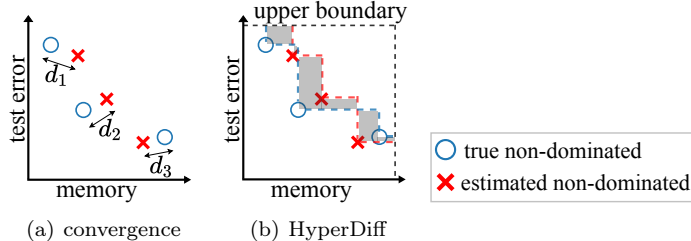


Figure 8: Illustration of Pareto frontier metrics. (a) Convergence is the average distance from each estimated Pareto optimal point to its closest true point: $\text{average}(d_1, d_2, d_3)$. (b) HyperDiff is the absolute difference in area of feasible regions given by the true and estimated Pareto optimal points: the shaded area between Pareto frontiers.

measurements on the new dataset by minimizing (a scalarization of) the variance,

$$\begin{aligned}
 & \text{minimize} && \log \det \left(\sum_{j \in S} y_j y_j^\top \right)^{-1} \\
 & \text{subject to} && |S| \leq l \\
 & && S \subseteq [d],
 \end{aligned} \tag{1}$$

to find S , the set of indices of configurations to evaluate. The positive integer l bounds the number of measurements. Given a memory cap m_{\max} , we replace the second constraint above by $S \subseteq T$, in which $T = \{j \in [d] \mid m_j^{\text{new}} \leq m_{\max}\}$ is the set of feasible configurations. Since Problem 1 is combinatorially hard, we may either relax it to a convex optimization problem by allowing decision variables to have non-integer values between 0 and 1, or use a greedy method to incrementally choose measurements (initialized by measurements chosen by the column-pivoted QR decomposition [25, 26]). We compare these two approaches in Appendix C.

In Section 4.2, we compare ED-MF with competing techniques and show it works the best to estimate the Pareto frontier and select the final configuration.

4 Experiments and discussions

The code for PEPPP and experiments is in the GitHub repository at <https://github.com/chengrunyang/peppp>. We use QPyTorch [27] to simulate low-precision formats on standard hardware.

The 87 datasets and 99 low-precision configurations in experiments are listed in Appendix A. The datasets consist of natural and medical images from various domains. Apart from CIFAR-10, the datasets include 20 CIFAR-100 partitions from mutually exclusive subsets, based on the superclass labels. They also include 50 subsets of ImageNet [18], which contains over 20,000 classes grouped into multiple major hierarchical categories like fungus and amphibian; each of the 50 datasets come from different hierarchies. Finally, we use 16 datasets from the visual domain benchmark [28] to increase the diversity of domains.

The 99 low-precision configurations use mixed-precision as described in Section 3.1. Format A (for the activations and weights) uses 5 to 9 bits; Format B (for the optimizer) ranges from 14 to 20 bits. For each, these bits may be split arbitrarily between the exponent and mantissa. Across all configurations, we use ResNet-18 with learning rate 0.001, momentum 0.99 and batch size 32. Each training uses only 10 epochs as an early stopping strategy [29] to prevent overfitting. All the measurements take 24 GPU days on NVIDIA[®] GeForce[®] RTX 2080 Ti.

Developing a method to select the above hyperparameters at the same time as the low-precision format is an important topic for future research, but not our focus here. In Section 4.3 we demonstrate how PEPPP can naturally extend to efficiently select both optimization and low-precision hyperparameters.

A number of metrics may be used to evaluate the quality of the obtained Pareto frontier in a multi-objective optimization problem [30, 31, 32]: the distance between approximated and true frontiers (convergence),

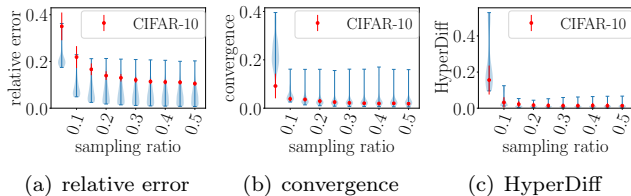
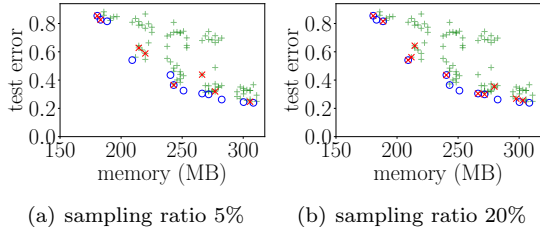


Figure 9: Pareto frontier estimation in PEPPP meta-training, with uniform sampling of configurations. The violins show the distribution of the performance on individual datasets, and the error bars (blue) show the range. The red error bars show the standard deviation of the error on CIFAR-10 across 100 random samples of the error matrix. Figure (a) shows the matrix completion error for each dataset; Figure (b) and (c) show the performance of the Pareto frontier estimates. Modest sampling ratios (around 0.1) already yield good performance.



(a) sampling ratio 5% (b) sampling ratio 20%

Figure 10: Error vs memory on CIFAR-10 with true and estimated Pareto frontiers from uniform sampling in PEPPP meta-training. A 20% uniform sample of entries yields a better estimate of the Pareto frontier (convergence 0.03 and HyperDiff 0.02) compared to a 5% sample (convergence 0.09 and HyperDiff 0.16).

the uniformity of the distances between neighboring Pareto optimal points (uniformity), how well the frontier is covered by the approximated points (spread), etc. In our setting, the memory is accurate and the test error is estimated, so we do not have full control of the uniformity and spread of the 2-dimensional frontiers between test error and memory. As illustrated in Figure 8, we evaluate the quality of our estimated Pareto frontiers by the following two metrics:

Convergence [33] between the set of true Pareto optimal points \mathcal{P} and estimated Pareto optimal points $\hat{\mathcal{P}}$ is $\frac{1}{|\hat{\mathcal{P}}|} \sum_{v \in \hat{\mathcal{P}}} \text{dist}(v, \mathcal{P})$, where the distance between point v and set \mathcal{P} is $\text{dist}(v, \mathcal{P}) = \min\{\|v - w\| : w \in \mathcal{P}\}$. This metric is a surrogate for the distance between Pareto frontiers.

Hypervolume difference (HyperDiff) [34, 35, 30] is the absolute difference between the volumes of solution spaces dominated by the true and estimated Pareto frontiers. This metric improves with better convergence, uniformity, and spread. Its computation requires an upper boundary for each resource.

When computing these metrics, we normalize the memories by proportionally scaling them to between 0 and 1. To evaluate the matrix completion performance, we use the relative error defined as $\|\hat{v} - v\|/\|v\|$, in which \hat{v} is the predicted vector and v is the true vector.

4.1 Meta-training

We study the effectiveness of uniform and non-uniform sampling schemes. For simplicity, we regard all 87 available datasets as meta-training in this section. In `SOFTIMPUTE`, we use $\lambda = 0.1$ (chosen by cross-validation from a logarithmic scale); and we choose a rank 5 approximation, which accounts for 78% of the variance in the error matrix (as shown in Figure 6(b)).

In the uniform sampling scheme, we investigate how many samples we need for accurate estimates: we sample the error matrix at a number of different ratios, ranging from 5% to 50%, and complete the error matrix from each set of sampled measurements. In uniform sampling, the sampling ratio is also the percentage of memory we need to make the measurements in parallel, compared to exhaustive search. Hence we show the relationship between Pareto frontier estimation performance and sampling ratio in Figure 9. We can see the estimates are more accurate at larger sampling ratios, but sampling 20% of the entries already suffices for good performance.

As a more intuitive example, Figure 10 shows the error-memory tradeoff on CIFAR-10. Compared to the estimated Pareto optimal points at sampling ratio 5%, the ones at 20% are closer to the true Pareto frontier (better convergence), lie more evenly (better uniformity) and cover the true Pareto frontier better (better spread), as shown by the respective convergence and HyperDiff values.

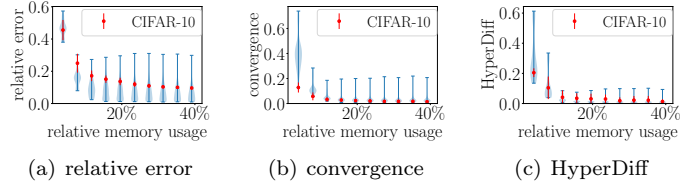


Figure 11: Pareto frontier estimation performance in PEPPP meta-training with non-uniform sampling of configurations. The violins and scatters have the same meaning as Figure 9. The x axis measures the memory usage relative to exhaustive search.

Table 1: Meta-LOOCV experiment settings

meta-training error matrix	memory cap on meta-test?	
	no	yes
full	I	II
uniformly sampled	III	IV
non-uniformly sampled	V	VI

In non-uniform sampling, we sample each entry of the error matrix E with probabilities $P_{ij} = \sigma(1/W_{ij})$, in which σ maps $\{1/W_{ij}\}$ into an interval $[0, p_{\max}] \subseteq [0, 1]$ according to the cumulative distribution function of $\{1/W_{ij}\}$. By varying p_{\max} , we change how we aggressively sample the configurations, how different the sampling probabilities are between large and small memory configurations, and also the percentage of memory needed. In Figure 11, we vary p_{\max} from 0.1 to 1 and see that the quality of the estimated Pareto frontier improves with more memory.

4.2 Meta-leave-one-out cross-validation (meta-LOOCV)

Now suppose that we have already collected measurements on the meta-training datasets to form a meta-training error matrix E (or its low rank approximation \hat{E}). On the meta-test dataset, PEPPP estimates the Pareto frontier by the active learning technique ED-MF. We compare ED-MF with a few other active learning techniques: RANDOM-MF, QR-MF, BO-MF and BO-FULL, to understand whether the strong assumptions in ED-MF (low rank and Gaussian errors) are a hindrance or a help.

- **Random selection with matrix factorization (RANDOM-MF)**. Same as ED-MF, RANDOM-MF predicts the unevaluated configurations by linear regression, except that it selects the configurations to evaluate by random sampling.
- **QR decomposition with column pivoting and matrix factorization (QR-MF)**. QR-MF first selects the configurations to evaluate by QR decomposition with column pivoting: $EP = QR$, in which the permutation matrix P gives the most informative configurations. Then it predicts unevaluated configurations in the same way as ED-MF and RANDOM-MF.
- **Bayesian optimization (BO)**. Bayesian optimization is a sequential decision making framework that learns and optimizes a black-box function by incrementally building surrogate models and choosing new measurements [36]. It works best for black-box functions that are expensive to evaluate and lack special structures or derivatives. We compare ED-MF with two BO techniques. The first technique, BO-MF, applies BO to the function $f_1 : \mathbb{R}^k \rightarrow \mathbb{R}$ that maps low-dimensional configuration embeddings $\{Y_{:,j}\}_{j=1}^d$ to the test errors of the configurations on the meta-test dataset $\{e_j^{\text{new}}\}_{j=1}^d$ [23]. The embeddings come from the same low-rank factorization of the error matrix E as in ED-MF. The second, BO-FULL, applies BO to the function $f_2 : \mathbb{R}^n \rightarrow \mathbb{R}$ that directly maps columns of the error matrix $\{E_{:,j}\}_{j=1}^d$ to $\{e_j^{\text{new}}\}_{j=1}^d$. To learn either of these black-box functions, we start by evaluating a subset of configurations $S \subseteq [d]$ and then incrementally select new configurations that maximize the expected improvement [37, 38].

We use rank 3 for matrix factorization: $Y_{:,j} \in \mathbb{R}^3$ for each $j \in [d]$. In BO, we tune hyperparameters on

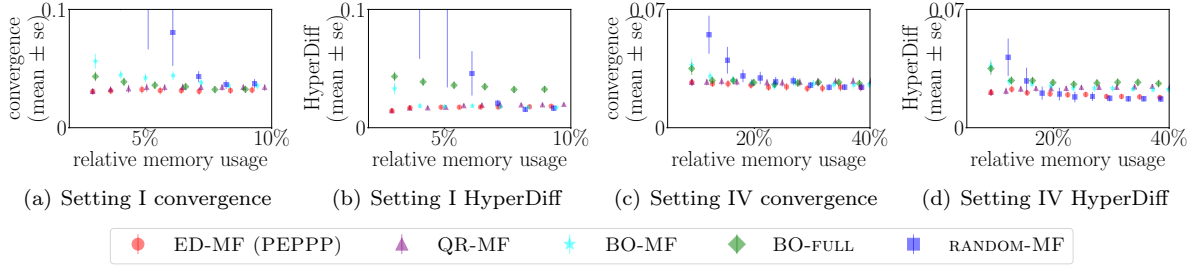


Figure 12: Pareto frontier estimates in meta-LOOCV Setting I and IV (with a 20% meta-training sampling ratio and an 816MB meta-test memory cap). Each error bar is the standard error across datasets. The x axis measures the memory usage relative to exhaustively searching the permissible configurations. ED-MF consistently picks the configurations that give the best PF estimates.

a logarithmic scale and choose the RBF kernel with length scale 20, white noise with variance 1, and $\xi = 0.01$. Table 1 shows the meta-LOOCV settings for each acquisition technique. We compare the techniques at a range of number of configurations to measure in each meta-LOOCV split, resembling what practitioners do in hyperparameter tuning: evaluate an informative subset and infer the rest. Setting I is the most basic, Setting IV and VI are the most practical. We only show results of Setting I and IV in the main paper, and defer the rest to Appendix D.

In Setting I, we do meta-LOOCV with the full meta-training error matrix in each split and do not cap the memory for meta-test. This means we evaluate every configuration on the meta-training datasets. We can see from Figure 12(a) and 12(b) that:

- ED-MF stably outperforms under both metrics, especially with fewer measurements.
- QR-MF overall matches the performance of ED-MF.
- BO-MF, BO-FULL and RANDOM-MF underperform ED-MF and QR-MF at lower memory usage, but often match their performance with higher memory.

Practitioners may have only collected part of the meta-training performance, and desire or are limited by a memory cap when they do meta-test on the new dataset. In Setting IV, we cap the single-configuration memory usage for meta-test at 816MB, the median memory of all possible measurements across configurations and datasets. Additionally, we uniformly sample 20% configurations from the meta-training error matrix in each split. In Figure 12(c) and 12(d), we can see similar trends as Setting I, except that QR-MF is slightly worse.

Ultimately, users would want to select a configuration that both achieves a small error and takes lower memory than the limit. As shown in Figure 2, PEPPP offers users the predicted Pareto frontier and chooses the non-dominated configuration with the highest allowable memory and hence the lowest error. We compare the acquisition techniques with the “random high-memory” baseline that randomly chooses a configuration that takes the highest allowable memory: an approach that follows the “higher memory, lower error” intuition. Figure 13 shows an example.

Overall, among all approaches and across all memory usage, ED-MF outperforms, especially at a smaller number of measurements. Compared to BO techniques, ED-MF also enjoys the benefit of having less hyperparameters to tune. Although techniques like QR-MF and RANDOM-MF are easier to implement, the additional cost of ED-MF is much smaller than the cost of making measurements: neural network training

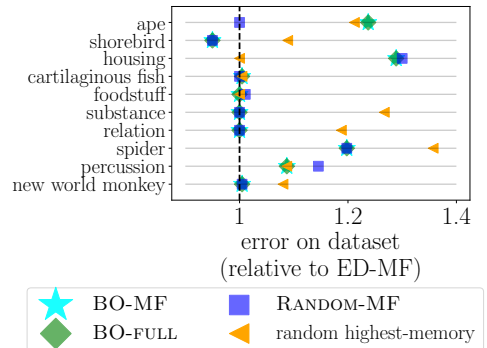


Figure 13: Relative performance with respect to ED-MF in meta-test Setting IV when making 3 measurements (memory usage $\sim 10\%$) on 10 ImageNet partitions. ED-MF outperforms in most cases.

and testing.

4.3 Tuning optimization hyperparameters

Previously, we have shown that PEPPP can estimate the error-memory tradeoff and select a promising configuration with other hyperparameters fixed. In practice, users may also want to tune hyperparameters like learning rate to achieve the lowest error. In Appendix D.2, we tune learning rate in addition to precision, and show that the methodology can be used to broader settings of hyperparameter tuning.

5 Conclusion

This paper proposes PEPPP, a meta-learning system to select low-precision configurations that leverages training information from related tasks to efficiently pick the perfect precision given a memory budget. Built on low rank matrix completion with active learning, PEPPP estimates the Pareto frontier between memory usage and model performance to find the best low-precision configuration at each memory level. By reducing the cost of hyperparameter tuning in low-precision training, PEPPP allows practitioners to efficiently train accurate models.

References

- [1] Roy Schwartz, Jesse Dodge, Noah A Smith, and Oren Etzioni. Green ai. *arXiv preprint arXiv:1907.10597*, 2019.
- [2] Christopher De Sa, Megan Leszczynski, Jian Zhang, Alana Marzoev, Christopher R Aberger, Kunle Olukotun, and Christopher Ré. High-accuracy low-precision training. *arXiv preprint arXiv:1803.03383*, 2018.
- [3] Nimit Sharad Sohoni, Christopher Richard Aberger, Megan Leszczynski, Jian Zhang, and Christopher Ré. Low-memory neural network training: A technical report. *arXiv preprint arXiv:1904.10631*, 2019.
- [4] Alex Krizhevsky, Geoffrey Hinton, et al. Learning multiple layers of features from tiny images. 2009.
- [5] Paulius Micikevicius, Sharan Narang, Jonah Alben, Gregory Diamos, Erich Elsen, David Garcia, Boris Ginsburg, Michael Houston, Oleksii Kuchaiev, Ganesh Venkatesh, et al. Mixed precision training. *arXiv preprint arXiv:1710.03740*, 2017.
- [6] Shuchang Zhou, Yuxin Wu, Zekun Ni, Xinyu Zhou, He Wen, and Yuheng Zou. Dorefa-net: Training low bitwidth convolutional neural networks with low bitwidth gradients. *arXiv preprint arXiv:1606.06160*, 2016.
- [7] Hantian Zhang, Jerry Li, Kaan Kara, Dan Alistarh, Ji Liu, and Ce Zhang. The zipml framework for training models with end-to-end low precision: The cans, the cannots, and a little bit of deep learning. *arXiv preprint arXiv:1611.05402*, 2016.
- [8] Matthieu Courbariaux, Yoshua Bengio, and Jean-Pierre David. Training deep neural networks with low precision multiplications. *arXiv preprint arXiv:1412.7024*, 2014.
- [9] Suyog Gupta, Ankur Agrawal, Kailash Gopalakrishnan, and Pritish Narayanan. Deep learning with limited numerical precision. In *International conference on machine learning*, pages 1737–1746. PMLR, 2015.
- [10] Christiane Lemke, Marcin Budka, and Bogdan Gabrys. Metalearning: a survey of trends and technologies. *Artificial intelligence review*, 44(1):117–130, 2015.
- [11] Joaquin Vanschoren. Meta-learning: A survey. *arXiv preprint arXiv:1810.03548*, 2018.
- [12] Timothy Hospedales, Antreas Antoniou, Paul Micaelli, and Amos Storkey. Meta-learning in neural networks: A survey. *arXiv preprint arXiv:2004.05439*, 2020.

- [13] Sara Hooker. The hardware lottery. *arXiv preprint arXiv:2009.06489*, 2020.
- [14] Zechun Liu, Haoyuan Mu, Xiangyu Zhang, Zichao Guo, Xin Yang, Kwang-Ting Cheng, and Jian Sun. Metapruning: Meta learning for automatic neural network channel pruning. In *Proceedings of the IEEE/CVF International Conference on Computer Vision*, pages 3296–3305, 2019.
- [15] Shangyu Chen, Wenya Wang, and Sinno Jialin Pan. Metaquant: Learning to quantize by learning to penetrate non-differentiable quantization. In *Advances in neural information processing systems*, pages 3916–3926, 2019.
- [16] Asit Mishra and Debbie Marr. Apprentice: Using knowledge distillation techniques to improve low-precision network accuracy. In *International conference on learning representations*, 2018.
- [17] Stephen Boyd and Lieven Vandenbergh. *Convex optimization*. Cambridge university press, 2004.
- [18] Jia Deng, Wei Dong, Richard Socher, Li-Jia Li, Kai Li, and Li Fei-Fei. ImageNet: A large-scale hierarchical image database. In *2009 IEEE Conference on Computer Vision and Pattern Recognition*, pages 248–255. IEEE, 2009.
- [19] Nimit Sharad Sohoni, Christopher Richard Aberger, Megan Leszczynski, Jian Zhang, and Christopher Ré. Low-memory neural network training: A technical report, 2019.
- [20] Rahul Mazumder, Trevor Hastie, and Robert Tibshirani. Spectral regularization algorithms for learning large incomplete matrices. *The Journal of Machine Learning Research*, 11:2287–2322, 2010.
- [21] Trevor Hastie, Rahul Mazumder, Jason D Lee, and Reza Zadeh. Matrix completion and low-rank svd via fast alternating least squares. *The Journal of Machine Learning Research*, 16(1):3367–3402, 2015.
- [22] Wei Ma and George H Chen. Missing not at random in matrix completion: The effectiveness of estimating missingness probabilities under a low nuclear norm assumption. In *Advances in Neural Information Processing Systems*, volume 32, pages 14900–14909, 2019.
- [23] Nicolo Fusi, Rishit Sheth, and Melih Elibol. Probabilistic matrix factorization for automated machine learning. In *Advances in neural information processing systems*, pages 3348–3357, 2018.
- [24] Chengrun Yang, Yuji Akimoto, Dae Won Kim, and Madeleine Udell. Oboe: Collaborative filtering for automl model selection. In *Proceedings of the 25th ACM SIGKDD International Conference on Knowledge Discovery & Data Mining*, pages 1173–1183, 2019.
- [25] Ming Gu and Stanley C Eisenstat. Efficient algorithms for computing a strong rank-revealing qr factorization. *SIAM Journal on Scientific Computing*, 17(4):848–869, 1996.
- [26] Gene H Golub and Charles F Van Loan. *Matrix computations*, volume 3. JHU press, 2012.
- [27] Tianyi Zhang, Zhiqiu Lin, Guandao Yang, and Christopher De Sa. Qpytorch: A low-precision arithmetic simulation framework, 2019.
- [28] Bram Wallace and Bharath Hariharan. Extending and analyzing self-supervised learning across domains. In *European Conference on Computer Vision*, pages 717–734. Springer, 2020.
- [29] Yuan Yao, Lorenzo Rosasco, and Andrea Caponnetto. On early stopping in gradient descent learning. *Constructive Approximation*, 26(2):289–315, 2007.
- [30] Jin Wu and Shapour Azarm. Metrics for quality assessment of a multiobjective design optimization solution set. *J. Mech. Des.*, 123(1):18–25, 2001.
- [31] Miqing Li, Shengxiang Yang, and Xiaohui Liu. Diversity comparison of Pareto front approximations in many-objective optimization. *IEEE Transactions on Cybernetics*, 44(12):2568–2584, 2014.
- [32] Charles Audet, Jean Bigeon, Dominique Cartier, Sébastien Le Digabel, and Ludovic Salomon. Performance indicators in multiobjective optimization. *European journal of operational research*, 2020.

- [33] Kalyanmoy Deb, Amrit Pratap, Sameer Agarwal, and TAMT Meyarivan. A fast and elitist multiobjective genetic algorithm: Nsga-ii. *IEEE Transactions on Evolutionary Computation*, 6(2):182–197, 2002.
- [34] Eckart Zitzler and Lothar Thiele. Multiobjective optimization using evolutionary algorithms—a comparative case study. In *International conference on parallel problem solving from nature*, pages 292–301. Springer, 1998.
- [35] Carlos A Coello Coello and Margarita Reyes Sierra. Multiobjective evolutionary algorithms: classifications, analyses, and new innovations. In *Evolutionary Computation*. Citeseer, 1999.
- [36] Peter I Frazier. A tutorial on bayesian optimization. *arXiv preprint arXiv:1807.02811*, 2018.
- [37] Jonas Moćkus. On bayesian methods for seeking the extremum. In *Optimization techniques IFIP technical conference*, pages 400–404. Springer, 1975.
- [38] Donald R Jones, Matthias Schonlau, and William J Welch. Efficient global optimization of expensive black-box functions. *Journal of Global optimization*, 13(4):455–492, 1998.
- [39] Stephen R Becker, Emmanuel J Candès, and Michael C Grant. Templates for convex cone problems with applications to sparse signal recovery. *Mathematical programming computation*, 3(3):165, 2011.
- [40] Vivek Madan, Mohit Singh, Uthaipon Tantipongpipat, and Weijun Xie. Combinatorial algorithms for optimal design. In *Conference on Learning Theory*, pages 2210–2258. PMLR, 2019.
- [41] Chengrun Yang, Jicong Fan, Ziyang Wu, and Madeleine Udell. Automl pipeline selection: Efficiently navigating the combinatorial space. In *Proceedings of the 26th ACM SIGKDD International Conference on Knowledge Discovery & Data Mining*, pages 1446–1456, 2020.
- [42] David A Harville. Matrix algebra from a statistician’s perspective, 1998.
- [43] Jack Sherman and Winifred J Morrison. Adjustment of an inverse matrix corresponding to a change in one element of a given matrix. *The Annals of Mathematical Statistics*, 21(1):124–127, 1950.

All the tables in this appendix are shown in the last page.

A Datasets and Low-Precision Formats

The 87 datasets chosen in our experiment are listed in Table 2. Note that the datasets contain images of two different resolutions: 32 denotes resolution $3 \times 32 \times 32$, and 64 denotes $3 \times 64 \times 64$. We list our choices of Format A and B in Table 3 and 4, respectively. In each evaluation, the low-precision configuration is composed of one Format A (for the activations and weights) and one Format B (for the optimizer), as detailed in Section 3.1. Therefore, the total number of low-precision configurations used in our experiment is 99.

B The SOFTIMPUTE Algorithm

There are several versions of SOFTIMPUTE; [21] gives a nice overview. We use the version in [20].

At a high level, SOFTIMPUTE iteratively applies a soft-thresholding operator \mathcal{S}_λ on the partially observed error matrix with a series of decreasing λ values. Each \mathcal{S}_λ replaces the singular values $\{\sigma_i\}$ with $\{(\sigma_i - \lambda)_+\}$. The regularization parameter λ can be set in advance or ad hoc, by convergence dynamics.

The pseudocode for the general SOFTIMPUTE algorithm is shown as Algorithm 1, in which $P_\Omega(E)$ is a matrix with the same shape as E , and has the (i, j) -th entry being E_{ij} if $(i, j) \in \Omega$, and 0 otherwise. In our implementation, $\lambda_i = \lambda t_i$ for each step i , and t_i is the step size from TFOCS backtracking [39].

Algorithm 1 SOFTIMPUTE

Input: a partially observed matrix $P_\Omega(E) \in \mathbb{R}^{n \times d}$, number of iterations I , a series of decreasing λ values $\{\lambda_i\}_{i=1}^I$

Output: an estimate \hat{E}

```

1 for  $i = 1$  to  $I$  do
2    $\tilde{E} \leftarrow P_\Omega(E) + P_{\Omega^c}(\hat{E})$ 
3    $U, \Sigma, V \leftarrow \text{svd}(\tilde{E})$ 
4    $\hat{E} \leftarrow U \mathcal{S}_\lambda(\Sigma) V^\top$ 

```

C Algorithms for Experiment Design

As mentioned in Section 3.2, there are mainly two algorithms to solve Problem 1, the D-optimal experiment design problem: convexification and greedy.

The convexification approach relaxes the combinatorial optimization problem to the convex optimization problem

$$\begin{aligned}
 & \text{minimize} && \log \det \left(\sum_{j=1}^d v_j y_j y_j^\top \right)^{-1} \\
 & \text{subject to} && \sum_{j=1}^d v_j \leq l \\
 & && v_j \in [0, 1], \forall j \in [d]
 \end{aligned} \tag{2}$$

that can be solved by a convex solver (like SLSQP). Then we sort the entries in the optimal solution $v^* \in \mathbb{R}^d$ and set the largest l entries to 1 and the rest to 0.

The greedy approach [40, 41] maximizes the submodular objective function by first choosing an initial set of configurations by column-pivoted QR decomposition, and then greedily adding new configuration to the solution set S in each step until $|S| = l$. The greedy stepwise selection algorithm is shown as Algorithm 2, in which the new configuration is chosen by the Matrix Determinant Lemma⁴ [42], and X_t^{-1} is updated

⁴The Matrix Determinant Lemma states that for any invertible matrix $A \in \mathbb{R}^{k \times k}$ and $a, b \in \mathbb{R}^k$, $\det(A + ab^\top) = \det(A)(1 + b^\top A^{-1}a)$. Thus $\operatorname{argmax}_{j \in [d] \setminus S} \det(X_t + y_j y_j^\top) = \operatorname{argmax}_{j \in [d] \setminus S} y_j^\top X_t^{-1} y_j$.

by the close form from the Sherman-Morrison Formula⁵ [43]. The column-pivoted QR decomposition selects top k pivot columns of $Y \in \mathbb{R}^{k \times d}$ to get the index set S_0 , ensuring that $X_0 = \sum_{j \in S_0} y_j y_j^\top$ is non-singular.

Algorithm 2 Greedy algorithm for D-optimal experiment design

Input: design vectors $\{y_j\}_{j=1}^d$, in which $y_j \in \mathbb{R}^k$; maximum number of selected configurations l ; initial set of configurations $S_0 \subseteq [d]$, s.t. $X_0 = \sum_{j \in S_0} y_j y_j^\top$ is non-singular

Output: the selected set of designs $S \subseteq [d]$

- 1 $S \leftarrow S_0$
 - 2 **while** $|S| \leq l$ **do**
 - 3 $i \leftarrow \operatorname{argmax}_{j \in [d] \setminus S} y_j^\top X_t^{-1} y_j$
 - 4 $S \leftarrow S \cup \{i\}$
 - 5 $X_{t+1} \leftarrow X_t + y_i y_i^\top$
-

The convexification approach empirically works because most entries of the optimal solution v^* are close to either 0 or 1. The histogram in Figure 14 shows an example when we use rank $k = 5$ to factorize the entire error matrix and set $l = 20$.

In terms of solution quality, the relative error plot in Figure 14 shows that the greedy approach consistently outperforms in terms of the relative matrix completion error for each dataset in ED-MF solutions. Since the greedy approach is also more than $10\times$ faster than convexification (implemented by `scipy`), we use the greedy approach throughout all experiments for the rest of this paper.

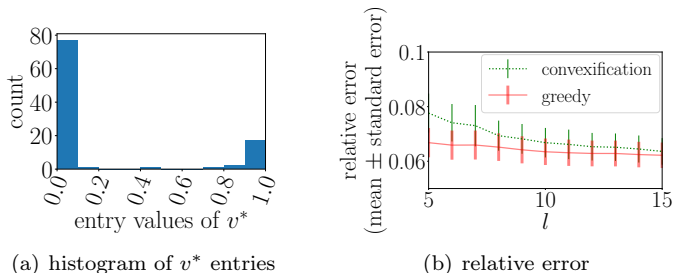


Figure 14: Convexification vs greedy for ED.

D Additional Experiments

We use the ratio of incorrectly classified images as our error metric. Figure 15 shows histograms of error and memory values in our error and memory matrices from evaluating 99 configurations on 87 datasets. The vertical dashed lines show the respective medians: 0.78 for test error and 816MB for memory. We can see both the test error and memory values span a wide range. The errors come from training a wide range of low-precision configurations with optimization hyperparameters not fine-tuned, and are thus larger than state-of-the-art results. In Section 4.3 of the main paper and Section D.2 here, we show that training for a larger number of epochs and with some other optimization hyperparameters yield the same error-memory tradeoff as Figure 1(a) in the main paper.

In meta-LOOCV settings with a meta-test memory cap at the median memory 816MB, Figure 16 shows a histogram of number of feasible configurations on each of the 87 datasets. There are “cheap” (resolution 32) datasets on which each of the 99 configurations takes less than the cap, and “expensive” (resolution 64) datasets on which the feasible configurations are far less than 99.

D.1 Additional Meta-LOOCV Results

In the main paper, we have shown the performance of Pareto frontier estimates and configuration selection for Setting I and IV. For the rest of the settings in Table 1, we conduct meta-LOOCV in the same way and show the results of Pareto frontier estimates in Figure 17.

⁵The Sherman-Morrison Formula states that for any invertible matrix $A \in \mathbb{R}^{k \times k}$ and $a, b \in \mathbb{R}^k$, $(A + ab^\top)^{-1} = A^{-1} - \frac{A^{-1}ab^\top A^{-1}}{1 + b^\top A^{-1}a}$.

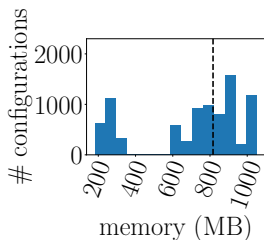
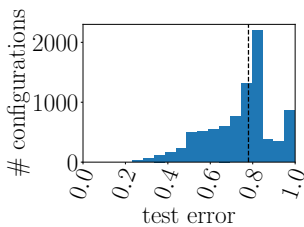


Figure 15: Histograms of error and memory. The dashed lines are the respective medians.

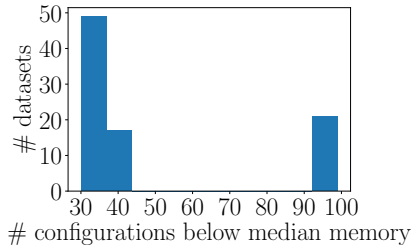


Figure 16: Histogram of datasets by the number of configurations that take memories less than the overall median of 816MB.

Setting II. We have the 816MB memory cap for meta-test, and have the full meta-training error matrix in each split.

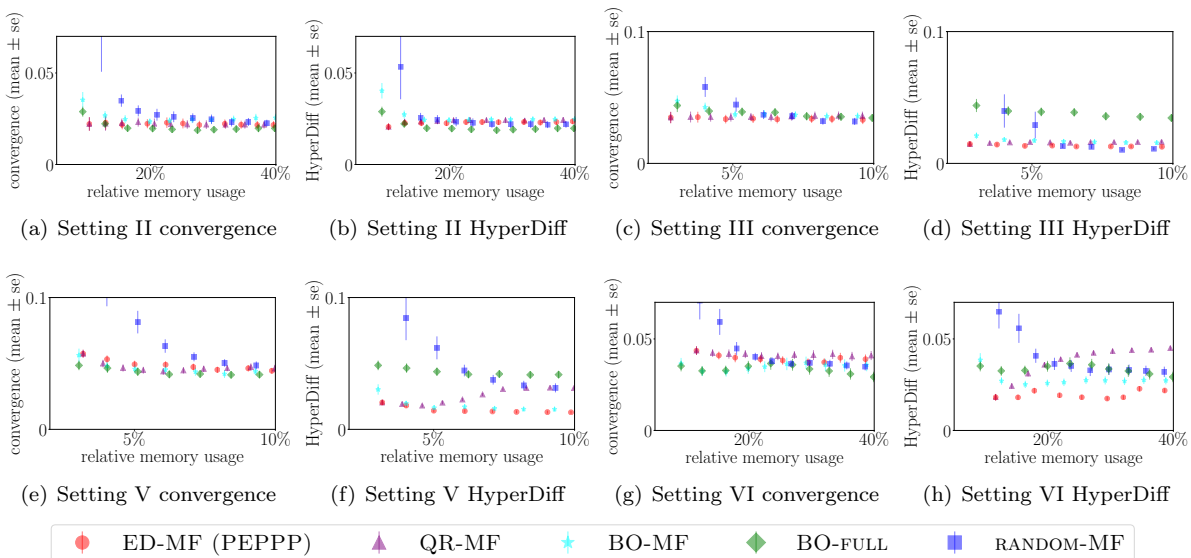


Figure 17: Pareto frontier estimates in meta-LOOCV Setting II (full meta-training error matrix, a 816MB memory cap), Setting III (uniformly sample 20% meta-training measurements, no meta-test memory cap), Setting V (non-uniformly sample 20% meta-training measurements, no meta-test memory cap), and Setting VI (non-uniformly sample 20% meta-training measurements, an 816MB meta-test memory cap). Each error bar is the standard error across datasets. ED-MF is among the best in every setting and under both metrics.

Setting III. We have no memory cap for meta-test, and uniformly sample 20% configurations for meta-training in each split.

Setting V. We have no memory cap for meta-test, and non-uniformly sample 20% configurations for meta-training in each split. The sampling method is the same as in meta-training (Figure 11).

Setting VI. We have the 816MB memory cap for meta-test, and non-uniformly sample 20% meta-training configurations in the same way as Setting V above.

D.2 Tuning Optimization Hyperparameters

Figure 18 shows that the error-memory tradeoff still exists with a fine-tuned learning rate for each configuration. With the learning rate tuned across $\{0.01, 0.001, 0.0001\}$, the test errors are in general

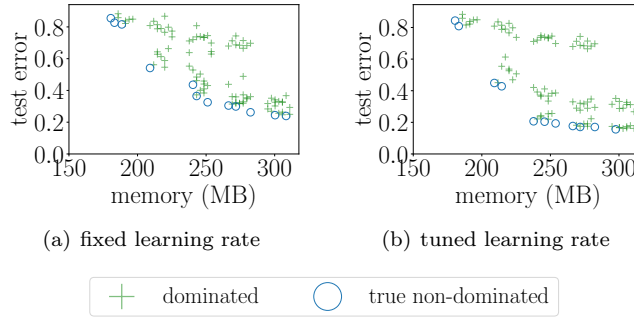


Figure 18: CIFAR-10 error-memory tradeoff. Figure (a) has learning rate 0.001 for all low-precision configurations. Figure (b) shows the tradeoff with tuned learning rates: at each low-precision configuration, the lowest test error achieved by learning rates $\{0.01, 0.001, 0.0001\}$ is selected.

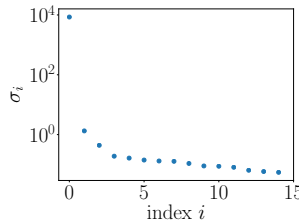


Figure 19: Singular value decay of the LR-tuned error matrix.

smaller, but high-memory configurations still achieve lower errors in general. Thus the need to efficiently select a low-precision configuration persists.

Our approach can naturally extend to efficiently selecting optimization *and* low-precision hyperparameters. We perform the meta-training and meta-LOOCV experiments on a subset of CIFAR-100 partitions with multiple learning rates $\{0.01, 0.001, 0.0001\}$. The error and memory matrices we use here have 45 rows and 99 columns, respectively. Learning rate and low-precision configuration are collapsed into the same dimension: each row corresponds to a combination of one CIFAR-100 subset and one of the learning rates $\{0.01, 0.001, 0.0001\}$, as shown in Table 5. We say that these error and memory matrices are *LR-tuned*. Figure 19 shows the LR-tuned error matrix also has a fast singular value decay. The other hyperparameters are the same as in LR-fixed experiments, except that we use batch size 128 and train for 100 epochs.

The meta-training and meta-LOOCV results are consistent with those in Sections 4.1 and 4.2, respectively.

In meta-training, we first uniformly sample the error matrix and study the performance of matrix completion and Pareto frontier estimation. Figure 20 shows the matrix completion error and Pareto frontier estimation metrics. Then we do non-uniformly sampling and get Figure 21, the LR-tuned version of Figure 11 in the main paper.

In meta-test, we evaluate settings in Table 1 in the main paper. We get the performance of Pareto frontier estimates in Figure 22, the LR-tuned version of Figure 12 in the main paper. ED-MF steadily outperforms.

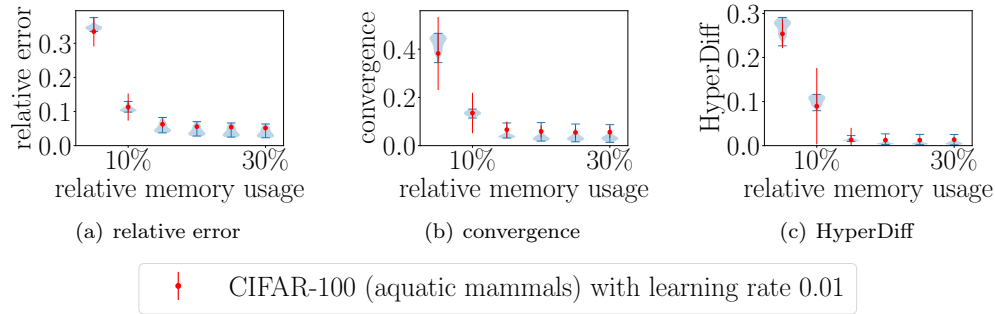


Figure 20: The Pareto frontier estimation performance in meta-training, with uniform sampling of configurations on the LR-tuned error and memory matrices. Similar to Figure 9, the violins show the distribution of the performance on individual datasets, and the error bars (blue) show the range. The red error bars show the standard deviation of the error on CIFAR-100 aquatic mammals and learning rate 0.01, across 100 random samples of the error matrix. Figure (a) shows the matrix completion error for each dataset; Figure (b) and (c) show the performance of the Pareto frontier estimates in convergence and HyperDiff.

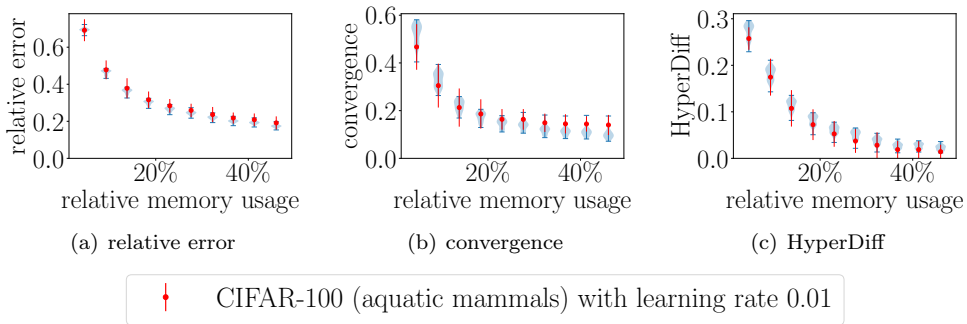


Figure 21: The Pareto frontier estimation performance in meta-training, with non-uniform sampling of configurations on the LR-tuned error and memory matrices. The violins and scatters have the same meaning as Figure 11 in the main paper.

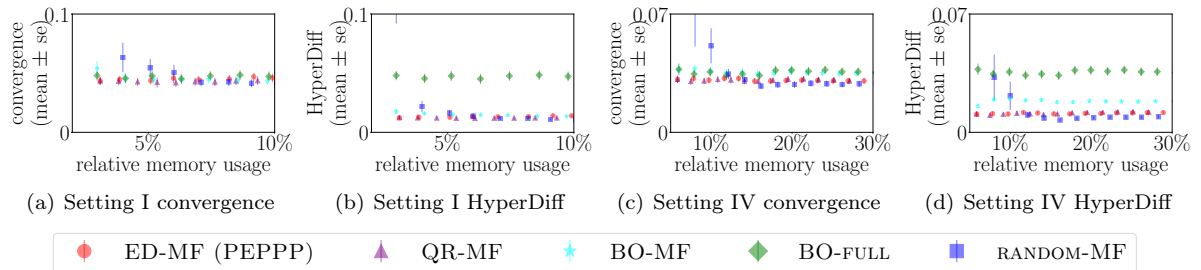


Figure 22: Pareto frontier estimates in meta-LOOCV settings on the LR-tuned error and memory matrices. Each error bar is the standard error across datasets.

Table 2: Datasets

index	dataset name	resolution	# points
1	CIFAR10	32	60000
2	CIFAR100 (aquatic mammals)	32	3000
3	CIFAR100 (fish)	32	3000
4	CIFAR100 (flowers)	32	3000
5	CIFAR100 (food containers)	32	3000
6	CIFAR100 (fruit and vegetables)	32	3000
7	CIFAR100 (household electrical devices)	32	3000
8	CIFAR100 (household furniture)	32	3000
9	CIFAR100 (insects)	32	3000
10	CIFAR100 (large carnivores)	32	3000
11	CIFAR100 (large man-made outdoor things)	32	3000
12	CIFAR100 (large natural outdoor scenes)	32	3000
13	CIFAR100 (large omnivores and herbivores)	32	3000
14	CIFAR100 (medium-sized mammals)	32	3000
15	CIFAR100 (non-insect invertebrates)	32	3000
16	CIFAR100 (people)	32	3000
17	CIFAR100 (reptiles)	32	3000
18	CIFAR100 (small mammals)	32	3000
19	CIFAR100 (trees)	32	3000
20	CIFAR100 (vehicles 1)	32	3000
21	CIFAR100 (vehicles 2)	32	3000
22	aircraft	64	6667
23	cub	64	10649
24	dtd	64	3760
25	isic	64	22802
26	merced	64	1890
27	scenes	64	14088
28	ucf101	64	12024
29	daimlerpedcls	64	29400
30	gtsrb	64	26640
31	kather	64	4000
32	omniglot	64	25968
33	svhn	64	73257
34	vgg-flowers	64	2040
35	bach	64	320
36	protein atlas	64	12113
37	minc	64	51750
38	ImageNet (bag)	64	6519
39	ImageNet (retriever)	64	6668
40	ImageNet (domestic cat)	64	6750
41	ImageNet (stick)	64	6750
42	ImageNet (turtle)	64	6750
43	ImageNet (finch)	64	6750
44	ImageNet (watchdog)	64	6404
45	ImageNet (footwear)	64	6587
46	ImageNet (salamander)	64	6750
47	ImageNet (anthropoid ape)	64	6750
48	ImageNet (elasmobranch)	64	6750
49	ImageNet (shorebird)	64	6750
50	ImageNet (housing)	64	6605
51	ImageNet (foodstuff)	64	6750
52	ImageNet (substance)	64	6643
53	ImageNet (spider)	64	8100
54	ImageNet (percussion instrument)	64	8082
55	ImageNet (New World monkey)	64	8100
56	ImageNet (big cat)	64	8100
57	ImageNet (box)	64	7829
58	ImageNet (fabric)	64	7862
59	ImageNet (kitchen appliance)	64	7773
60	ImageNet (mollusk)	64	8100
61	ImageNet (hand tool)	64	8054
62	ImageNet (butterfly)	64	8100
63	ImageNet (stringed instrument)	64	8100
64	ImageNet (boat)	64	8006
65	ImageNet (rodent)	64	8006
66	ImageNet (toiletry)	64	7522
67	ImageNet (computer)	64	7696
68	ImageNet (shop)	64	9400
69	ImageNet (musteline mammal)	64	9450
70	ImageNet (Old World monkey)	64	9450
71	ImageNet (bottle)	64	9205
72	ImageNet (fungus)	64	9450
73	ImageNet (truck)	64	9309
74	ImageNet (spaniel)	64	9119
75	ImageNet (sports equipment)	64	9450
76	ImageNet (game bird)	64	9450
77	ImageNet (seat)	64	9126
78	ImageNet (fruit)	64	9450
79	ImageNet (weapon)	64	9450
80	ImageNet (beetle)	64	10800
81	ImageNet (toy dog)	64	9832
82	ImageNet (decapod crustacean)	64	10800
83	ImageNet (fastener)	64	10675
84	ImageNet (timepiece)	64	10164
85	ImageNet (dish)	64	10556
86	ImageNet (mechanical device)	64	10617
87	ImageNet (colubrid snake)	64	12150

Table 3: Format A (for activations and weights)

index	# exponent bits	# mantissa Bits	total bit width
1	3	1	5
2	3	2	6
3	3	3	7
4	3	4	8
5	4	1	6
6	4	2	7
7	4	3	8
8	4	4	9
9	5	1	7
10	5	2	8
11	5	3	9

Table 4: Format B (for optimizer)

index	# exponent bits	# mantissa Bits	total bit width
1	6	7	14
2	6	9	16
3	6	11	18
4	7	7	15
5	7	9	17
6	7	11	19
7	8	7	16
8	8	9	18
9	8	11	20

Table 5: Datasets and learning rates in Section 4.3

index	dataset name	learning rate
1	CIFAR100 (aquatic mammals)	0.01
2	CIFAR100 (fish)	0.01
3	CIFAR100 (flowers)	0.01
4	CIFAR100 (food containers)	0.01
5	CIFAR100 (fruit and vegetables)	0.01
6	CIFAR100 (household electrical devices)	0.01
7	CIFAR100 (household furniture)	0.01
8	CIFAR100 (insects)	0.01
9	CIFAR100 (large carnivores)	0.01
10	CIFAR100 (large man-made outdoor things)	0.01
11	CIFAR100 (large natural outdoor scenes)	0.01
12	CIFAR100 (large omnivores and herbivores)	0.01
13	CIFAR100 (medium-sized mammals)	0.01
14	CIFAR100 (non-insect invertebrates)	0.01
15	CIFAR100 (people)	0.01
16	CIFAR100 (reptiles)	0.01
17	CIFAR100 (aquatic mammals)	0.001
18	CIFAR100 (fish)	0.001
19	CIFAR100 (flowers)	0.001
20	CIFAR100 (food containers)	0.001
21	CIFAR100 (fruit and vegetables)	0.001
22	CIFAR100 (household electrical devices)	0.001
23	CIFAR100 (household furniture)	0.001
24	CIFAR100 (insects)	0.001
25	CIFAR100 (large carnivores)	0.001
26	CIFAR100 (large man-made outdoor things)	0.001
27	CIFAR100 (large natural outdoor scenes)	0.001
28	CIFAR100 (large omnivores and herbivores)	0.001
29	CIFAR100 (medium-sized mammals)	0.001
30	CIFAR100 (non-insect invertebrates)	0.001
31	CIFAR100 (people)	0.001
32	CIFAR100 (reptiles)	0.001
33	CIFAR100 (aquatic mammals)	0.0001
34	CIFAR100 (fish)	0.0001
35	CIFAR100 (flowers)	0.0001
36	CIFAR100 (food containers)	0.0001
37	CIFAR100 (fruit and vegetables)	0.0001
38	CIFAR100 (household electrical devices)	0.0001
39	CIFAR100 (household furniture)	0.0001
40	CIFAR100 (insects)	0.0001
41	CIFAR100 (large carnivores)	0.0001
42	CIFAR100 (large man-made outdoor things)	0.0001
43	CIFAR100 (large natural outdoor scenes)	0.0001
44	CIFAR100 (large omnivores and herbivores)	0.0001
45	CIFAR100 (medium-sized mammals)	0.0001